

Synthesis of Electrochemically Active LiMnPO_4 via $\text{MnPO}_4 \cdot \text{H}_2\text{O}$ with Different Morphology Prepared By Facile Precipitation

Li Wang, Wenting Sun, Jiangjun Li, Jian Gao, Xiangming He*, Changyin Jiang

Institute of Nuclear and New Energy Technology, Beijing Key Lab of Fine Ceramics, Tsinghua University, Beijing 100084, PR China

*E-mail: hexm@tsinghua.edu.cn

Received: 24 January 2012 / Accepted: 5 March 2012 / Published: 1 April 2012

$\text{MnPO}_4 \cdot \text{H}_2\text{O}$ is successfully prepared with different morphology by facile precipitation. The various morphologies of $\text{MnPO}_4 \cdot \text{H}_2\text{O}$ can be fabricated with different reaction conditions such as reaction temperature, reaction concentration, solvents and stirring time. The synthesized $\text{MnPO}_4 \cdot \text{H}_2\text{O}$ is further used as the precursor to prepare LiMnPO_4 . XRD, SEM and TG/DSC are performed to characterize as-prepared samples. The capacity can reach 106mAh g^{-1} after carbon coating. This paves a facile way to prepare LiMnPO_4 for Li-ion batteries.

Keywords: LiMnPO_4 ; $\text{MnPO}_4 \cdot \text{H}_2\text{O}$; morphology; precipitation; lithium ion battery

1. INTRODUCTION

The Lithium-Ion Battery has attracted wide attention due to its increased market demand for portable electronics, transportation and energy storage. Olivine framed lithium metal phosphates such as LiMPO_4 (M=Fe, Mn) have been extensively investigated as advanced cathode materials due to their low cost, low toxicity and thermal stability [1, 8]. LiMnPO_4 has higher theoretical energy density ($684 \text{Wh/kg} = 171 \text{mAh g}^{-1} \times 4.0 \text{V}$) than LiFePO_4 ($578 \text{Wh kg}^{-1} = 170 \text{mAh g}^{-1} \times 3.4 \text{V}$) because of the ideal location of the $\text{Mn}^{2+}/\text{Mn}^{3+}$ couple at 4.1 V vs Li/Li^+ , which is $\sim 0.65 \text{V}$ higher than LiFePO_4 [9]. But the high ionic and electronic resistances of LiMnPO_4 have limited its performance release.

Encouraged by the successful attempts on LiFePO_4 , designing LiMnPO_4 in the nano-scale region can be an effective way to reduce the diffusion path length to improve the performance of LiMnPO_4 [10-13]. It offers potential for high electrode/electrolyte surface contact to improve the rate capability. Several reports from HPL research group have demonstrated that particle size reduction is essential to improve the rate performance of the LiMnPO_4 materials. For instance, LiMnPO_4 with

140nm-200nm size distribution are synthesized by sol-gel method, which enhanced the reversible capacity to 156 mAh g^{-1} at $C/100$ and 134 mAh g^{-1} at $C/10$ [14]. Their collaborators also prepared a platelet-like LiMnPO_4 with thickness around 25 nm, which had excellent electrochemical performance [15]. Hence, LiMnPO_4 with the plate-like shape and nano-scale size distribution attracted much attention as they may provide short pathway for the Li ion diffusion. D. Choi et al. synthesized LiMnPO_4 nanoplates with a thickness of 50 nm that are assembled and grew into nanorods along the [010] direction in the (100) plane [16]. This improved the reversible capacity as high as 168 mAh g^{-1} at $C/50$, which is close to the theoretical value. Yang et al. synthesized LiMnPO_4 nanoplates with carbon coating, its capacity reached to be 147 mAh g^{-1} [17]. Thus, it is evident that rapid and effective methods for preparing nano-scale LiMnPO_4 materials are essential.

However, above mentioned preparations are to synthesize nano- LiMnPO_4 directly, which is difficult to control the morphology and size distribution. Recently, the preparation based on favorable precursor is attractive as it allows the regulation of morphology and orientation of the formed precursor which can be consistent with the final product. Xiao et al. synthesized LiMnPO_4 from a $\text{MnPO}_4 \cdot \text{H}_2\text{O}$ precursor exhibits a discharge capacity of 115 mAh g^{-1} at $C/20$ rate as its best electrochemical performance [18]. In this study, we synthesized various morphology of nano- $\text{MnPO}_4 \cdot \text{H}_2\text{O}$ precursor under different conditions by chemical precipitation process. On that basis, nano- LiMnPO_4/C with good electrochemical performance is prepared and tested.

2. EXPERIMENTAL

$\text{MnPO}_4 \cdot \text{H}_2\text{O}$ is prepared by a facile precipitation as follows. A stoichiometric amount of $\text{Mn}(\text{NO}_3)_2$ and H_3PO_4 are dissolved in the solvent. The preparation procedure is carried out under stirring at different conditions with details in Table 1. After the reaction, powders are washed with water and ethanol before dried in a vacuum oven at $60 \text{ }^\circ\text{C}$. Nano- LiMnPO_4 is prepared by solid-state carbothermal reduction. $\text{MnPO}_4 \cdot \text{H}_2\text{O}$ is mixed with a stoichiometric amount of $\text{LiCOOCH}_3 \cdot 2\text{H}_2\text{O}$ and 10% sucrose in the agate mortar. Then the mixture is calcined at 500°C for 4 h in flowing ultra-pure Ar or N_2 to obtain nano- LiMnPO_4 material.

Table 1. Details about different conditions for preparing $\text{MnPO}_4 \cdot \text{H}_2\text{O}$ and the corresponding LiMnPO_4

Precursor	50% $\text{Mn}(\text{NO}_3)_2$	85% H_3PO_4	$\text{C}_2\text{H}_5\text{OH}$	H_2O	Tempe rature	Stirrin g Time	Final Product
MnPO_4 -1	0.08mol	20ml	80ml	0	70°C	2h	LiMnPO_4 - a
MnPO_4 -2	0.16mol	20ml	80ml	0	RT	2h	LiMnPO_4 - b
MnPO_4 -3	0.08mol	20ml	70ml	10ml	RT	2h	LiMnPO_4 - c
MnPO_4 -4	0.08mol	20ml	80ml	0	RT	6h	LiMnPO_4 - d

X-ray diffraction pattern (XRD, D/max 2550V, Rigaku, Japan) with Cu-K α irradiation ($\lambda=1.5406$ nm) are used to characterize the products. The morphology of the samples is inspected using scanning electron microscope (SEM, JSM-5600LV, JEOL, Japan) and transmission electron microscope (TEM, H-800, Hitachi, Japan). We use a combined differential scanning calorimetry/thermogravimetric analysis (DSC/TGA) instrument (Netzsch, STA 449C) to study the decomposition and reaction of the precursors. The MnPO₄ powder and the mixed starting materials for preparing LiMnPO₄ are heated in argon to 900°C at the rate of 5°C/min for DSC/TGA analysis.

A composite electrode used for electrochemical test is prepared by mixing LiMnPO₄/C composite, acetylene black and poly (vinylidene fluoride) (PVDF) with weight ratio of 8:1:1. Lithium metal is used as the counter electrode. The electrolyte is a 1 M LiPF₆/EC(ethylene carbonate)+DMC(dimethyl carbonate)+DEC(diethyl carbonate) (3:3:1 by volume) and the separator is Celgard 2500. The CR2032 cell is assembled in the glove box filled with highly pure argon gas. The charge/discharge performance is tested between 3.0 and 4.5 V at a constant current (2.5 mA g⁻¹) at room temperature.

3. RESULTS AND DISCUSSION

The XRD patterns for as-prepared MnPO₄·H₂O precursor are shown in Fig.1. All the samples are well crystallized in monoclinic system. The diffraction lines in the XRD patterns are in agreement with standard MnPO₄·H₂O (JCPDS NO.44-0071).

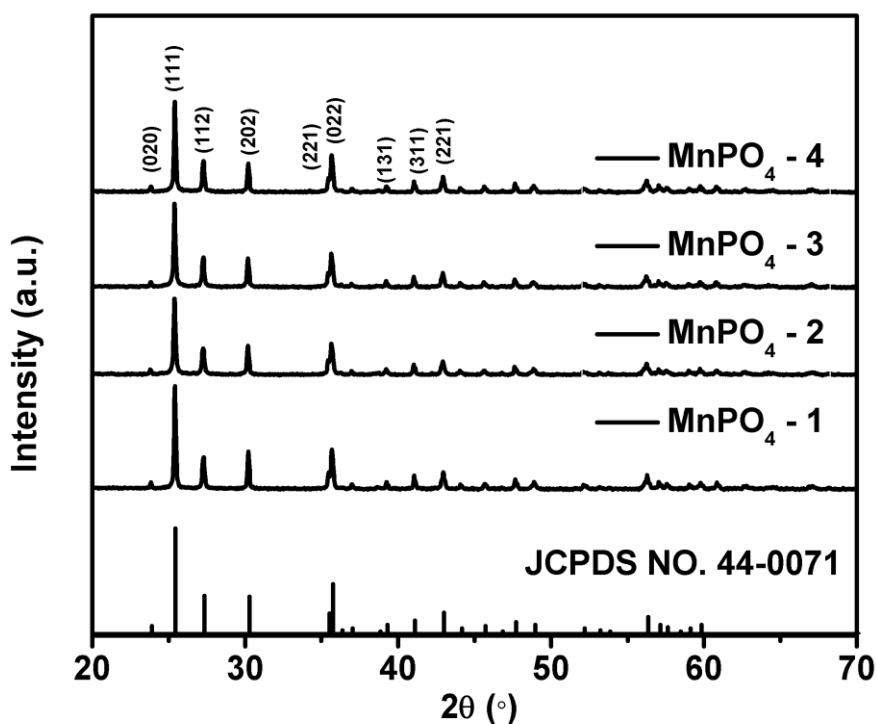


Figure 1. XRD patterns of MnPO₄·H₂O synthesized at different conditions.

No characteristic lines of impurity phases are observed, indicating the high purity of the samples. Generally, $\text{MnPO}_4 \cdot \text{H}_2\text{O}$ can be easily precipitated at room temperature, only if high acidity can be satisfied since oxidization of Mn^{2+} to Mn^{3+} by NO_3^- can happen only in high acidity conditions [18, 19]. But in the precipitation, the reaction rate is hardly controlled, that caused random morphology and wide size distribution. So we design four different experiment conditions so as to get uniform nano-sized $\text{MnPO}_4 \cdot \text{H}_2\text{O}$ particles with favorable morphology. The effect of temperature, concentration, addition of water and time of stirring in the chemical precipitation process are discussed next.

The varied morphology of as-prepared $\text{MnPO}_4 \cdot \text{H}_2\text{O}$ samples synthesized at different conditions are shown in Fig.2. From the SEM images, it can be observed that all the samples consist of secondary particles which are random in shape. These secondary particles are formed by loose aggregation of primary particles which also have different shapes. It proved that the chemical precipitation process can strongly effect the crystal growth and the final morphology.

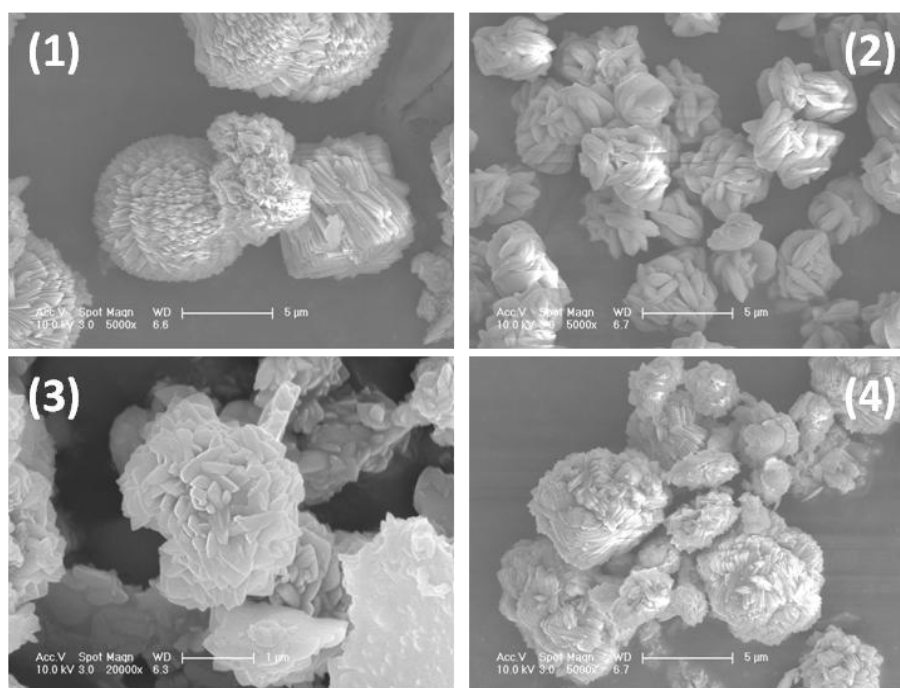


Figure 2. SEM photographs of $\text{MnPO}_4 \cdot \text{H}_2\text{O}$ synthesized at different conditions. [(1) MnPO_4 -1; (2) MnPO_4 -2; (3) MnPO_4 -3; (4) MnPO_4 -4]

For MnPO_4 -1 sample, the secondary particles are accumulated by nano-plates with different size, and show narrow size distribution (5 μm -6 μm). This is attributed to the high reaction temperature to get uniform nano-plates. But high temperature also leads to the tightly accumulated nano-plates which is unfavorable in the successive synthesis and carbon coating. Therefore, high concentration of the starting material is adopted at room temperature instead of at high temperature. This makes preparation simple. The synthesized secondary particles which have a uniform size distribution of 4 μm can be observed in Fig.2 (2). They are consisted of several primary rice-shaped particles with regular

morphology and the size distribution of 2 μ m long and 400nm wide. Compared with other samples, it is obvious that this sample has larger primary particles but smaller secondary particles. In general, particle size increases with increase of reactant concentration [20]. This provides reasonable explanation for the larger primary particles. The growth of MnPO₄·H₂O crystal determines the size of primary particles at current condition. The micron size distribution may appropriately decrease the aggregation compared with nano materials. Otherwise, ethanol is used as inert solvents that may reduce the formation of secondary particles. Therefore, a certain amount of deionized water is added to ethanol as the mixed solvent to be used for synthesis of the third sample. As shown in Fig.2 (3), the sample with nano-sized thin flakes is successfully synthesized. These thin flakes has a narrow size distribution of 300-400nm and aggregated as micron-sized secondary particles. It can be seen that time of stirring had little effect to the morphology of the products from Fig.2 (4).

As reported, MnPO₄·H₂O is a good candidate precursor for LiMnPO₄ preparation, since the crystal structure of MnPO₄·H₂O is close to that of LiMnPO₄ [9, 18]. The difference between them is that hydrogen ions reside in the tunnels of MnPO₄·H₂O structure instead of lithium ions in LiMnPO₄. This allows a transformation from MnPO₄·H₂O into LiMnPO₄ without major structural rearrangements. As a result, the size distribution and morphology of LiMnPO₄ can be easily controlled by designing those of MnPO₄·H₂O.

Before the synthesis of LiMnPO₄ from the precursor, it is important to know the exact amount of water in the MnPO₄·H₂O precursor, as it influences the final stoichiometry of the final LiMnPO₄ product [21]. And the thermal behaviors of the mixed starting materials containing MnPO₄·H₂O, LiAc and sucrose are essential to get the annealing program for LiMnPO₄ preparation. All above information can be obtained from TG/DSC curves of MnPO₄·H₂O powders and the mixed starting materials for LiMnPO₄ under argon in Fig.3. According to Fig.3 (A), the two steps in TG curve are consistent with the two DSC endothermic peaks, which are attributed to the release of partial crystallization water and the reduction of manganese (III) to manganese (II), and the consequent release of oxygen and remanent crystallization water of MnPO₄·H₂O, respectively. The corresponding temperature and weight loss coincide with the reports in literatures [22, 23], indicating that thermal decomposition reaction as happened as follows:



The weight loss of the sample calculated in the curves based on Fig.3 (A) is 15.6%, which is coincided with the theoretical weight loss of 15.48% according to the reaction including 4.76% from O₂ and 10.72% from H₂O. Moreover, the second endothermic peak in DSC curve around 479.1 $^{\circ}$ C present the appearance of Mn₂P₂O₇, nearly 40 $^{\circ}$ C lower than macro size bulk MnPO₄·H₂O. It is benefit to decrease the annealing temperature for nano-MnPO₄·H₂O materials when compared with macro size bulk MnPO₄·H₂O materials.

Fig. 3(B) shows TG/DSC curves of the mixed starting materials for LiMnPO₄. As been shown, the decomposition process occurs in the temperature interval from 50 to 350 $^{\circ}$ C with a total weight loss of 41%. There are several sharp endothermic peaks at temperatures less than 300 $^{\circ}$ C in the DSC curve, which is attributed to the dehydration and thermal decomposition of LiAc and sucrose. As

is known, the reaction of generating stable compound will release heat. The exothermic peak at 456.2°C in the DSC curve indicates the formation of LiMnPO₄. And we get the important information that annealing temperature at about 500°C may be appropriate to promote the crystalline growth of LiMnPO₄.

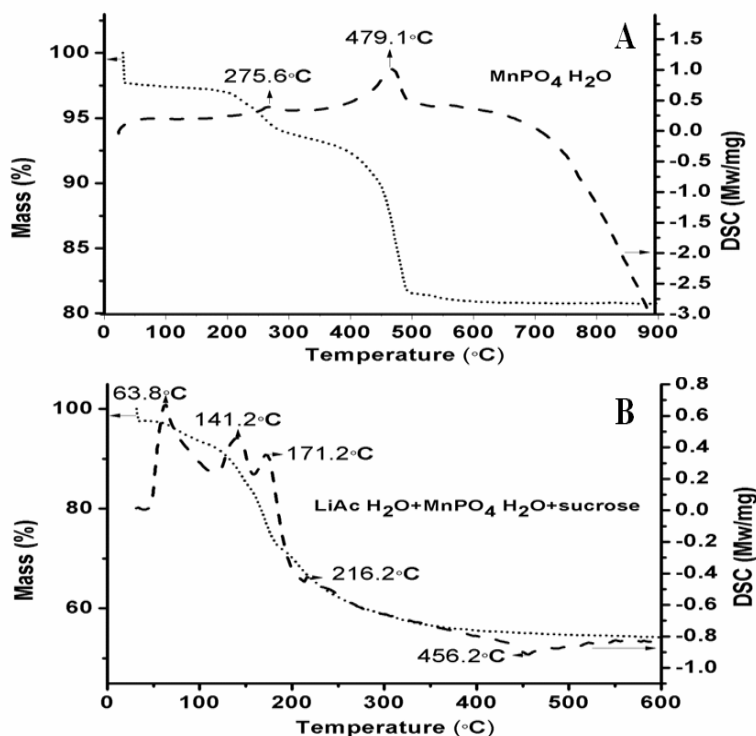


Figure 3. TG/DSC curves of MnPO₄·H₂O-3 powders (A) and the mixed starting materials for LiMnPO₄ (B) under argon.

The XRD patterns of as-prepared LiMnPO₄ and the corresponding varied MnPO₄·H₂O precursors are shown in Fig. 4. All the diffraction lines in the patterns are in agreement with standard LiMnPO₄ (JCPDS NO. 33-0803), which is olivine structure indexed in *Pnma* of an orthorhombic system. No characteristic lines of impurity phase are observed, indicative of the purity of the samples, since the presence of the MnPO₄·H₂O precursor can significantly reduce the impurities like Li₃PO₄ which usually forms in the direct precipitation and calcination process [24]. The coated carbon in the LiMnPO₄/C cannot be detected in the XRD patterns because of its small amount. Fig.5 shows SEM images of LiMnPO₄ powders which are synthesized using varied MnPO₄ precursor. We can get the information that the basic morphology of secondary particles of the precursor is maintained. The sample (LiMnPO₄ -a) is consisted of some dispersed spheres with size distribution between 5μm and 6μm, which is as same as its MnPO₄·H₂O precursor. The carbon coating on the surface can be observed clearly. But the morphology of nano-plates cannot be clearly seen because of the coating. The secondary particles with uniform size distribution are shown in Fig.5 (b). After carbon coating and calcining, the final products are still uniform but denser than before. Compared with the morphology of precursor, the micron-sized secondary particles disappear in Fig.5 (c). The images show uniform

size distribution of the final LiMnPO_4/C products with nano-sized primary particles which have homogeneous carbon coating. As shown in Fig.5, morphologies of the final products are similar to those of the corresponding precursors. The aggregation is observed after carbon coating and annealing process.

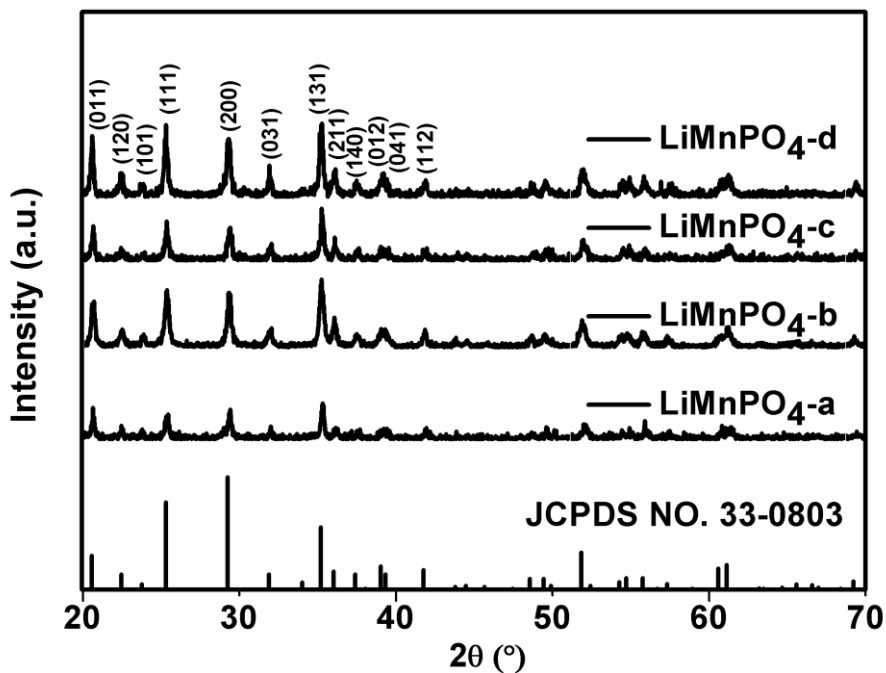


Figure 4. XRD patterns of LiMnPO_4 powders.

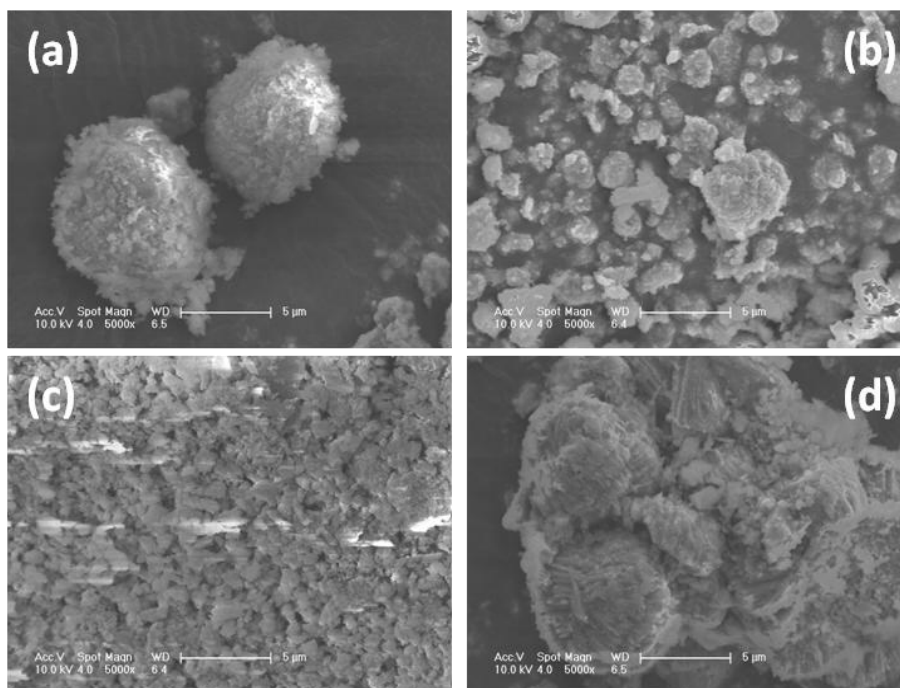


Figure 5. SEM photographs of LiMnPO_4 powders from the corresponding MnPO_4 precursor. [(a) LiMnPO_4 -a; (b) LiMnPO_4 -b; (c) LiMnPO_4 -c; (d) LiMnPO_4 -d]

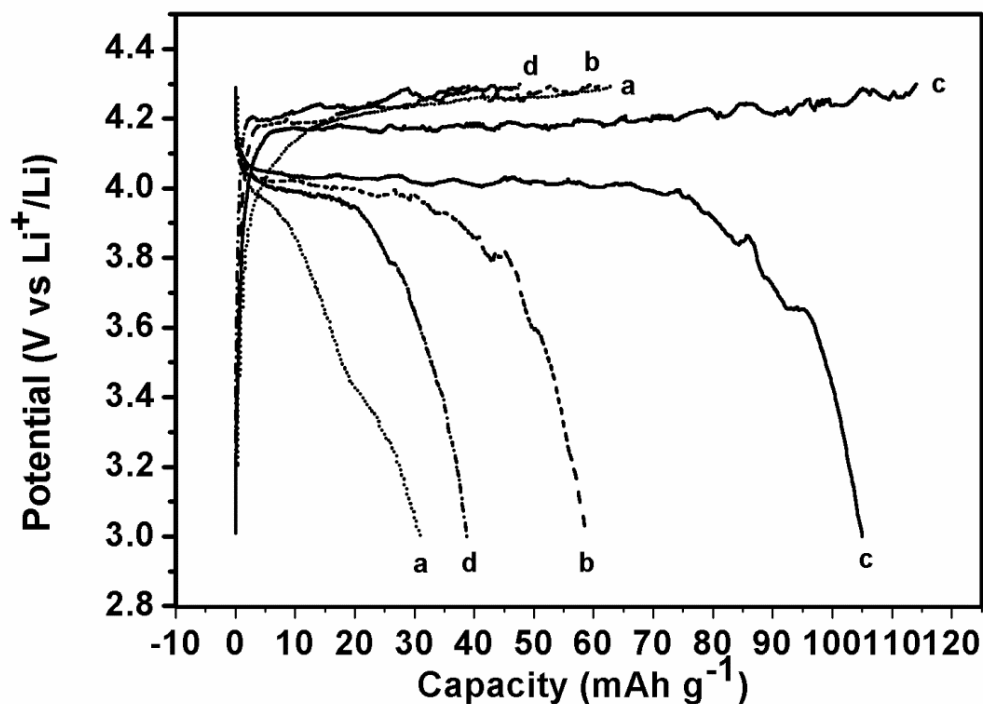


Figure 6. Charge-discharge curves of LiMnPO_4/C powders.

The differences in morphologies and dispersity between $\text{MnPO}_4 \cdot \text{H}_2\text{O}$ precursor and LiMnPO_4/C powder are owing to carbon coating originated from sucrose during the annealing process. It is hard to seep into the precursor for sucrose with dense accumulated secondary particles in the sample (a) and (d). This leads to non-uniform carbon coating, which affects the electrochemical performance due to its electronic conductivity improved by carbon coating. So the method to obtain homogenous carbon coating needs to be explored in the further investigation.

The charge–discharge curves of LiMnPO_4/C powders which are synthesized using varied MnPO_4 precursor are shown in Fig.6. The cells are cycled between 3 and 4.3V at a constant current density of 2.5 mA g^{-1} . As can be seen in Fig. 6, the cathode clearly exhibits electrochemical activity with charge and discharge plateaus around the voltage of 4.1V vs. Li^+/Li . These plateaus correspond to the redox of $\text{Mn}^{3+}/\text{Mn}^{2+}$ that accompanies with lithium ion extraction and insertion in LiMnPO_4 . But both the sample (a) and the sample (d) which have similar morphologies of the precursors and carbon coatings exhibit poor reversible capacities and large irreversible capacities during the first cycle. As above discussion, low electronic conductivity which has not been improved by the morphology and carbon coating leads to poor electrochemical performance. The sample (b) and (c) have good reversible capacities during the first cycle. Improved electrochemical performance of the sample (b) is probably attributed to uniform morphology of the final LiMnPO_4/C powders. As expected, the sample (c) exhibits the best electrochemical performance among all the samples. The smooth charge and discharge plateaus bring in good reversible capacity which can achieve 106mAh/g. This is because the uniform size distribution of the final LiMnPO_4/C products with nano-sized primary particles which have homogeneous carbon coating. All the favorable factors for electrochemical performance are achieved in the sample (c) with the precursor sample (MnPO_4 -3).

4. CONCLUSION

MnPO₄·H₂O materials are successfully prepared with different morphologies by a simple precipitation method. High temperature and long stirring time in the precipitation process of precursor can benefit for the formation of nano-plates but densely accumulated which is hard to react with Li salt and sucrose. Large primary particles with rice-like shape but small secondary particles can be obtained by the high concentration. Nano-sized thin flakes with size distribution of 300-400nm are successfully synthesized in the mixed solvent containing ethanol and water. The best electrochemical performance among the as-prepared LiMnPO₄/C samples can achieve 106mAh/g with nano-sized thin flakes and homogeneous carbon coating. All above results demonstrate that electrochemically active LiMnPO₄ can be obtained by this proposed method, which use morphology-controlled MnPO₄·H₂O as the precursor. The electrochemical performance can be improved by optimizing the morphology of precursor and carbon coating.

ACKNOWLEDGEMENT

This work is supported by the Ministry of Science and Technology (Grant No. 2011CB935902 and Grant No. 2010DFA72760), the National Natural Science Foundation of China (Grand No.20901046 and Grand No.20903061) and the Tsinghua University Initiative Scientific Research Program (Grand No. 2010THZ08116, No.2011THZ08139 and No.2011THZ01004).

References

1. J. Gao, J.J Li, X.M. He, C.Y. Jiang, C.R. Wan, *Int. J. Electrochem. Sci.*, 6(2011)2818-2825.
2. D. Bhuvanewari, Gangulibabu, Chil-Hoon Doh, N. Kalaiselvi, *Int. J. Electrochem. Sci.*, 6(2011)3714-3728.
3. Y. Lin, Y.B. Lin, B.Z. Zeng, G.Y. Zhao, T. Zhou, M.L. Chen, X.M. Mao, H. Lai, Z.G. Huang, *Int. J. Electrochem. Sci.*, 6(2011)6653-6661.
4. H.-C. Wong, J. R. Carey, J.-S. Chen, *Int. J. Electrochem. Sci.*, 5(2010)1090-1102.
5. C.L. Hu, H.H. Yi, H.S. Fang, B. Yang, Y.C. Yao, W.H.i Ma, Y.N. Dai, *Int. J. Electrochem. Sci.*, 5(2010)1457-1463.
6. Gangulibabu, N. Kalaiselvi, D. Bhuvanewari, C. H. Doh, *Int. J. Electrochem. Sci.*, 5(2010)1597-1604.
7. C. Delacourt, P. Poizot, M. Morcrette, J. M. Tarascon, C. Masquelier, *Chem. Mater.* 16 (2004) 93-99.
8. H.H Yi, C.L. Hu, H.H. Fang, B. Yang, Y.C. Yao, W.H Ma, Y.N. Dai. *Int. J. Electrochem. Sci.*, 7(2012)663-670.
9. L. Wang, W. T. Sun, X. M. He, J. J. Li, C. Y. Jiang, *Int. J. Electrochem. Sci.* 6 (2011) 2022-2030.
10. H. Huang, S. C. Yin, L. F. Nazar, *Electrochem. Solid-State Lett.* 4 (2001) A170-A172.
11. S. Y. Chung, J. T. Bloking, Y. M. Chiang, *Nat. Mater.* 1 (2002) 123-128.
12. A. Vadivel Murugan, T. Muraliganth, A. Manthiram, *J. Phys. Chem. C.* 112 (2008) 14665-14671.
13. B. Ellis, Wang Hay Kan, W. R. M. Makahnouk, L. F. Nazar, *J. Mater. Chem.* 17 (2007) 3248-3254.
14. T. Drezen, N. H. Kwon, P. Bowen, I. Teerlinck, M. Isono, I. Exnar, *J. Power Sources* 174 (2007) 949-953.
15. S. K. Martha, B. Markovsky, J. Grinblat, Y. Gofer, O. Haik, E. Zinigrad, D. Aurbach, T. Drezen, D. Wang, G. Deghenghi, I. Exnar, *J. Electrochem. Soc.* 156 (2009) A541-A552.

16. D. W. Choi, D. H. Wang, I. T. Bae, J. Xiao, Z. M. Nie, W. Wang, V. V. Viswanathan, Y. J. Lee, J. G. Zhang, G. L. Graff, Z. G. Yang, J. Liu, *Nano Lett.* 10 (2010) 2799–2805.
17. F. Wang, J. Yang, P. F. Gao, Y. N. NuLi, J. L. Wang, *J. Power Sources* 196 (2011) 10258-10262.
18. J. Xiao, W. Xu, D. W. Choi, J. G. Zhang, *J. Electrochem. Soc.* 157 (2010) A142-A147.
19. Y. K. Sun, S. M. Oh, H. K. Park, B. Scrosati, *Adv. Mater.* 23 (2011) 5050-5054.
20. D. Rangappa, K. Sone, M. Ichihara, T. Kudo, I. Honma, *Chem. Commun.* 46 (2010) 7548-7550.
21. B. Boonchom, R. Baitahe, Z. P. Joungmunkong, N. Vittayakorn, *Powder Tech.* 203 (2010) 310–314.
22. B. Boonchom, S. Youngme, S. Maensiri, C. Danvirutai, *J. Alloys Compd.* 454 (2008) 78-82.
23. T. Witzke, R. Wegner, T. Doering, H. Pollmann, W. Schuckmann, *American Mineralogist*, 85 (2000) 847-849.
24. H. Fang, Z. Pan, L. Li, Y. Yang, G. Yan, G. Li, S. Wei, *Electrochem. Commun.* 10 (2008) 1071-1073.